From snow accumulation to snow depth distributions by quantifying meteoric ice ~~fractions~~ in the Weddell Sea

Stefanie Arndt[1], Nina Maaß[1,2], Leonard Rossmann[1], Marcel Nicolaus[1]

[1]Alfred-Wegener-Institut Helmholtz-Zentrum für Polar- und Meeresforschung, 27570 Bremerhaven, Germany
5   [2] Center for Earth System Research and Sustainability, University of Hamburg, 20146 Hamburg, Germany

Correspondence to: Stefanie Arndt (stefanie.arndt@awi.de)

Abstract. A year-round snow cover is a characteristic of Antarctic sea ice, which has significant implications for the energy and mass budgets of sea ice, e.g., by preventing surface melt in summer and enhancing sea ice growth through extensive snow ice formation. However, substantial observational gaps in the seasonal cycle of Antarctic sea ice and its snow cover limit the

10   understanding of important processes in the ice-covered Southern Ocean. They also introduce large uncertainties in satellite remote sensing applications and climate studies.

Here we present results from 10 years of autonomous snow observations from Snow Buoys in the Weddell Sea. To distinguish between actual snow depth and potential snow ice thickness within the accumulated snowpack, a one-dimensional thermodynamic sea ice model is applied along the drift trajectories of the buoys. The results show that for 44% of the analyzed

15   Snow Buoy tracks snow ice formation with an average thickness of 35 cm was detected, which corresponds to about one quarter of the snow accumulation. In addition, we simulate the snow accumulation with the more complex SNOWPACK model, which results in superimposed ice thicknesses between 2 and 9 cm. These estimates will provide an important reference dataset for both snow depth and meteoric ice rates in the Southern Ocean.

20   **Short summary.** Antarctic sea ice maintains year-round snow cover, crucial for its energy and mass budgets. Despite its significance, snow depth remains poorly understood. Over the last decades, Snow Buoys have been deployed extensively on the sea ice to measure snow accumulation but not actual depth due to snow transformation into meteoric ice. Therefore, in this study, we utilize sea ice and snow models to estimate meteoric ice fractions in order to calculate actual snow depth in the Weddell Sea.

25   **1 Introduction**

The role of the snow cover is particularly intriguing for the understanding of sea ice mass budget in the Southern Ocean, as Antarctic snow cover survives potential summer melt and persists during most of the year (Massom et al., 2001). The low thermal conductivity makes snow an effective insulator, and thus dampens the thermodynamic ice growth at the bottom (Calonne et al., 2011; Sturm et al., 1997). It also contributes to ice growth from the top through the formation of meteoric ice

30 (Eicken et al., 1994). Snow-to-ice conversion processes, i.e., snow ice and superimposed ice formation, are instrumental in comprehending this complex system. Snow ice results from the submergence of ice beneath the snow/ice interface, facilitated by heavy snow loads (e.g., Eicken et al., 1994; Tian et al., 2020). Subsequent flooding and refreezing of the snow/water mixture result in the creation of this unique ice form, a process that is particularly pronounced during the winter months. In contrast, the formation of superimposed ice is driven by internal melting within the snowpack during summer as snowmelt water

35 percolates downward and refreezes at the snow/ice interface (Ackley et al., 2008; Nicolaus et al., 2009; Haas and Eicken, 2001; Arndt et al., 2021).

In addition to its direct effects, snow also hampers the interpretation and retrieval of sea ice parameters, including thickness and volume of sea ice observed using in-situ and with satellite remote sensing. The conversion of either ice draft, measured by means of upward looking sonars, or ice freeboard, measured by means of satellite altimetry (Ricker et al., 2015; Fons and

40 Kurtz, 2019; Kwok et al., 2020), into ice thickness, depends heavily on reliable snow depth and density data. As the ratio of snow load to ice thickness is particularly high for Antarctic sea ice, the snow cover has a significant effect on the freeboard of Antarctic sea ice (Worby et al., 2008). Consequently, the estimation of ice thickness is particularly reliant on the conversion of freeboard to thickness, resulting in significant uncertainty in Antarctic sea ice thickness retrievals (Paul et al., 2018; Kwok and Kacimi, 2018; Schwegmann et al., 2016).

45 Despite the fact, that snow depth on sea ice is such an essential state variable of the polar climate system, it is yet one of the least known parameters in the Antarctic sea ice systems (Webster et al., 2018). However, attempts have been made to describe it at different spatial scales. Therefore, it is imperative to distinguish between the terminologies of snow accumulation and snow depth since the two may not always correspond due to the various snow conversion processes outlined previously. Snow accumulation refers to all the snow that has fallen at a certain location during a specified period of time. Snow depth (or

50 thickness), in turn, describes the actual amount of snow present at a specific location and time, which results from the difference between snow accumulation and the thickness of meteoric ice formed up to that point in time.

MagnaProbe measurements, for example, can be used to determine snow depth at a certain point in time at a certain location (Sturm and Holmgren, 2018). To extend these point measurements to larger spatial and temporal scales, Snow Buoys have been developed. These are autonomous measuring systems deployed on the sea ice and measure, among other things, hourly

55 snow accumulation rates along the drift and transmit them via satellite link (Nicolaus et al., 2021). However, these ice-tethered platforms cannot describe the potential conversion processes of snow into meteoric ice at the snow/ice interface. As a result, snow accumulation from Snow Buoys cannot be taken as a direct measure of snow depth.

To bridge this gap and finally get a first approximation of snow depth distributions in the Weddell Sea for different regions and seasons, this study uses a simple thermodynamic sea ice model to quantify snow ice formation along the trajectories of

60 Snow Buoys in the Weddell Sea over the last decade. In addition, the snow model SNOWPACK is utilized to estimate

superimposed ice formation along the same trajectories. The resulting snow and superimposed layer thicknesses are validated with in-situ observations in the southeastern and northwestern Weddell Sea in recent years.

Given that different ice classes experience different contributions from these processes, the reduction in uncertainties varies across the Antarctic sea ice cover. Nevertheless, the results presented reveal distinct variations between regions and seasons,

65   providing a pathway towards improved snow depth datasets. This improvement, in turn, has the potential to reduce uncertainties in sea ice thickness data products derived from satellite remote sensing and sea ice modelling applications.

2 Data and methods
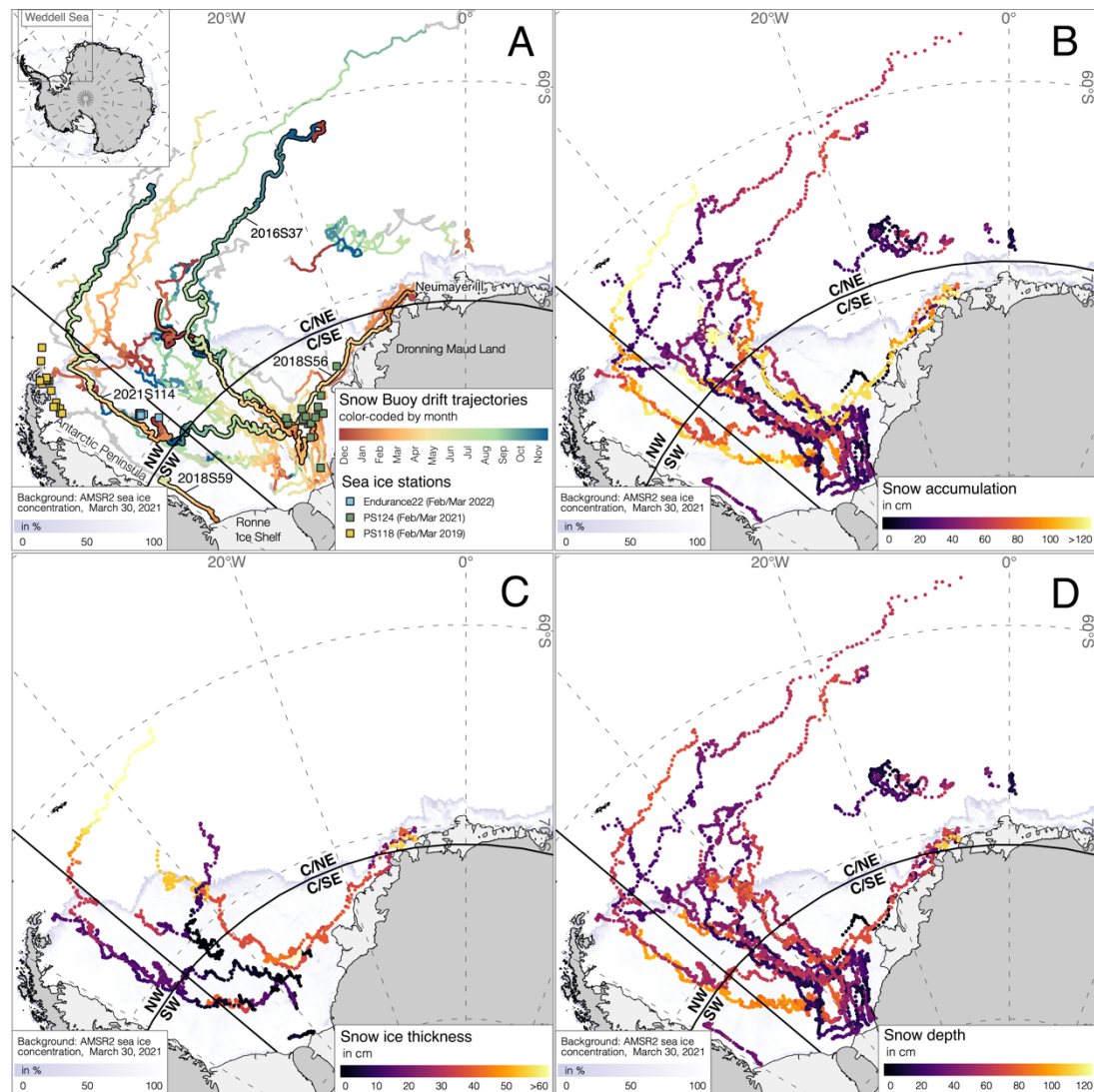
Figure 1. A Map of all Snow Buoy drift trajectories since 2013 in the Weddell Sea. The trajectories are color-coded by month

70   for the time of valid snow accumulation data. Further buoy drifts without valid snow accumulation data are marked in gray.

The black-margined trajectories highlight the paths of the Snow Buoys 2016S37, 2018S56, 2018S59 and 2021S114. They are examples of the defined drift patterns in the Weddell Sea (e.g., Chapter 3.1). Colored squares mark additional ice station data from the given expeditions that complement the Snow Buoy data. **B** Snow accumulation measured from the Snow Buoys along their drift trajectory. **C** Estimated snow ice thickness from the one-dimensional thermodynamic ice growth model and **D**

75   resulting calculated snow depth. For all panels: Solid black lines mark the four separated regions: southwestern (SW), northwestern (NW), central/ southeastern (C/SE), central/ northeastern (C/NE) Weddell Sea. Background: AMSR2 sea ice concentration from March 30, 2021 (Spreen et al., 2008).

2.1 Study area

The Weddell Sea features a distinctive large-scale cyclonic circulation pattern, the Weddell Gyre, which is driven primarily
80   by mean atmospheric geostrophic forcing (Vernet et al., 2019). This circulation, combined with wind stress, influences surface ocean currents, resulting in an inflow of sea ice in the eastern region and an outflow in the northwest. Within this drift, parts of the sea ice cover survive the summer melt and eventually become second year ice. Drift dynamics, coupled with the pronounced seasonality of the ice cover, contribute to the predominance of seasonal ice in the eastern Weddell Sea and promote the formation of polynyas, particularly along the coast of the Ekström Ice Shelf and the Filchner-Ronne Ice Shelf (e.g., Paul
85   et al., 2015). As a result, sea ice reaches maximum thicknesses of up to 1.5 m near the coast of Dronning Maud Land, while second year ice in the southwestern and western regions can reach thicknesses exceeding 3 m, representing some of the thickest sea ice in the Southern Ocean (Haas et al., 2008; Harms et al., 2001).

For the purposes of this study, the Weddell Sea has been divided into four regions (Figure 1A). Region I includes the compact perennial sea ice of the southwestern Weddell Sea, south of 71°S and west of 50°W. Region II covers the northwestern Weddell
90   Sea, including the predominantly perennial sea ice and the western marginal ice zone, located north of 71°S and west of 50°W. Region III corresponds to the highly dynamic central and southeastern Weddell Sea, characterized by predominantly seasonal sea ice, south of 71°S and east of 50°W. Finally, Region IV represents the central and eastern Weddell Sea marginal sea ice zone, consisting of both seasonal and perennial sea ice, located north of 71°S and east of 50°W.

2.2 Snow Buoys

95   Snow Buoys are autonomous measuring systems hourly recording snow accumulation under four ultra-sonic sensors as well as air temperature and barometric air pressure. Given the height of the sensor mast, a maximum snow accumulation of 1.50 m can be recorded. The systems are deployed on sea ice and transmit their data via satellite connection. For more technical details, see Nicolaus et al. (2021). For this study, all Snow Buoys deployed between 2013 and 2022 on drifting pack ice in the Weddell Sea (27 buoys) or on the fast ice in Atka Bay (9 buoys), close to the German overwintering base Neumayer Station III (Arndt
100   et al., 2020), are considered (Figure 1A). As the Snow Buoys in the Weddell Sea were deployed during ship-based expeditions,

which usually take place in austral summer, most time series start between December and February. All snow accumulation values of the individual Snow Buoys are presented as a daily average of all four ultra-sonic sensors. Monthly accumulation (ablation) rates are then calculated as the sum of the positive (negative) changes in these daily values over each month.

Here we use the buoy's names, as introduced in Nicolaus et al. (2021), consisting of the deployment year, the buoy type 'S',
105 and a serial counter (Grosfeld et al., 2015).

2.3 One-dimensional thermodynamic sea ice model

A simple one-dimensional thermodynamic ice growth model based on the number of freezing degree days (Thorndike, 1992), as used in Arndt et al. (2021), is applied to estimate the evolution of the thermodynamic sea ice growth at the bottom of the ice and the resulting ice freeboard. For the latter, a simplified assumption is made that a calculated negative freeboard causes
110 potential flooding of the snow/ice interface and subsequent snow-to-ice conversion, i.e., snow ice formation, both taking place in the same time step.

Model runs are initialized with the measured initial sea ice thickness during buoy deployment. The atmospheric forcing of the model, i.e., surface temperature and heat fluxes, is based on ERA5 reanalysis data (Copernicus Climate Change Service, 2017), while the ocean is prescribed with a constant oceanic heat flux of 3 Wm^{-2} (Robertson et al., 1995). ERA5 reanalysis data were
115 extracted for the nearest-neighbor grid points of the daily buoy positions. For snow density and thermal conductivity regionally adjusted parameters following Arndt (2022) are applied.

2.4 Multi-layer snow model SNOWPACK

To estimate the amount of both snow ice and superimposed ice formed during the buoys' lifetime, we use the multi-layer snow cover model SNOWPACK. In the one-dimensional SNOWPACK model, snow microstructure is represented in detail and
120 liquid water flow and refreezing processes are taken into account (Bartelt and Lehning, 2002; Lehning et al., 2002a; Lehning et al., 2002b; Wever et al., 2015; Wever et al., 2016). SNOWPACK was originally developed to represent physical processes in the snow cover in alpine regions, but has been adapted and applied to sea ice environments recently (Wever et al., 2021; Wever et al., 2020).

For our simulations, we initialize the model with the initial snow and ice thicknesses as measured during buoy deployment.
125 For the general model setup, the layers' initial salinity and volumetric contents of air, ice and water (corresponding to the layers' density), we follow the approach of Wever et al. (2021). However, for the atmospheric stability, we chose the approach following Holtslag and De Bruin (1988), as in the SNOWPACK model documentation this was changed to be the new default setting (the effect on the snow depth is minor). Like in the simple thermodynamic sea ice model described above, the atmospheric forcing is based on ERA5 reanalysis data. Here, we present snow-height-driven simulations, which means that
130 the SNOWPACK simulations are forced to closely follow the snow height evolution as measured by the Snow Buoy. While

snow accumulation as indicated in the Snow Buoy datasets will lead to an instant increase in the SNOWPACK simulation (like a precipitation event), sudden reductions in snow height will only be incorporated within the scope of the model physics. Wind-induced transport of snow is neglected, and the ocean heat flux is set to a constant value of 5 Wm^{-2}. The ocean heat flux of both models differs. This is a result of different sensitivities of the models to the heat flux. In both cases, the best results

135 after sensitivity studies were used (data not shown here). The simulated snow densities are used to distinguish between snow (density ≤ 600 kg m^{-3}), superimposed ice (600 kg m^{-3} < density < 918 kg m^{-3}) and snow ice (density ≥ 918 kg m^{-3}).

2.5 In-situ data of snow and ice properties

To provide a comprehensive context for the Snow Buoy measurements and to validate the results of the one-dimensional thermodynamic sea ice model (Section 2.3), additional ice station work conducted during expeditions to the Weddell Sea in

140 the late austral summer, i.e., February and March, is presented (Figure 1A). The ice station work during expedition PS124 of the German icebreaker *RV Polarstern* in 2021 focused on the southeastern Weddell Sea (Haas et al., 2021). In contrast, the ice stations of expedition PS118 (Haas et al., 2019), also conducted by *RV Polarstern*, and the expedition Endurance22, carried out with the South African icebreaker *S.A. Agulhas II* (Rabenstein, 2022), covered the northwestern Weddell Sea. During these expeditions, snow depth was measured using a GPS-equipped Magna Probe (Snow Hydro, Sturm and Holmgren

145 (2018)) along transect lines spanning several kilometers across the entire sampled ice floes. Additional analyses of ice cores, focusing on salinity and stable water isotopes, were performed to determine the fractions of superimposed ice and snow ice (e.g., Arndt et al., 2021).

3 Results and Discussion

3.1 Drift regimes in the Weddell Sea

150 As described in Section 2.1, a significant proportion of the sea ice in the Weddell Sea forms in the polynyas along the east coast and is subsequently transported north(-west) wards by the Weddell Gyre. In addition, the seasonal fast ice near Atka Bay drifts along its eastern coast into the Weddell Sea (e.g., Snow Buoy 2018S56). However, closer examination of the ice drift patterns reveals variations in the drift regimes (Figure 1A) (Schwegmann et al., 2011). Some of the sea ice floes formed in the southeastern Weddell Sea follow a rather pronounced northward trajectory, ending up in the marginal ice zone of the central

155 and eastern Weddell Sea (e.g., 2016S37, Figure 1A). Other ice floes form in the southeastern Weddell Sea drift on a longer southerly course, eventually ending up in the northwestern Weddell Sea (e.g., 2021S114, Figure 1A). However, the exact location of their origin along the eastern Weddell Sea coast and their subsequent drift trajectories do not have a clear geographical assignment. Instead, these trajectories are more influenced by geostrophic winds (Kottmeier et al., 1992), local sea ice/ocean/shelf ice interactions causing currents (Kottmeier and Sellmann, 1996), tides (Robertson et al., 1998), as well as

160 the sea ice thickness and concentration (Vihma et al., 1996).

In addition, polynyas in the southern Weddell Sea, including the Ronne Polynya, also produce persistent sea ice (Haas et al., 2008). This ice is frequently transported westward by the Weddell Gyre, which then carries it north along the Antarctic Peninsula towards the northwestern Weddell Sea (e.g., 2018S59).

165 Considering the literature cited and the diverse drift trajectories observed for the Snow Buoys (Figure 1A), it is reasonable to assume that these buoys ~~accurately~~ capture the prevailing drift patterns in the Weddell Sea. Therefore, the snow analyses conducted along the buoys' drift trajectories, as presented below, can be regarded as representative for the region as a whole.

3.2 Spatial and seasonal variability of snow accumulation rates
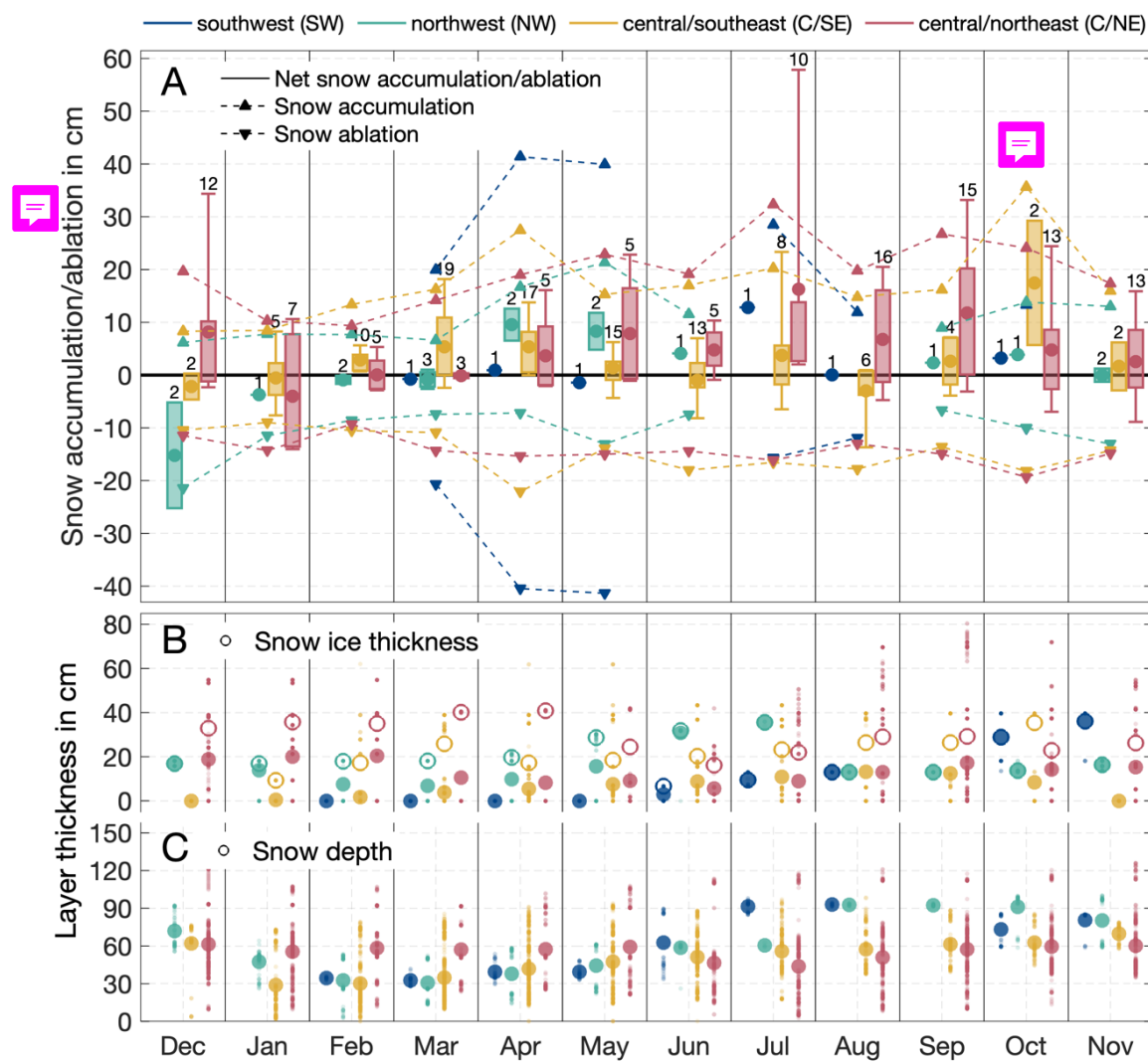
Figure 2. A Monthly mean snow accumulation rates (upward triangles), snow ablation (downward triangle), and net
accumulation (positive) or ablation (negative) rates (boxplots) of all Snow Buoys separated for the four regions in the Weddell
Sea (see Figure 1). Data were included if at least 25 days per cycle were available in the respective month and region. Numbers
indicate the amount of annual buoy cycles contributing to the mean value. In the boxplots, boxes span over the first and third
quartiles. The whiskers display the 10th and 90th percentiles; the circles indicate mean values, which may include contributions
from both accumulation and ablation. Panels **B** and **C** display the calculated layer thicknesses of snow ice and snow,
respectively, from the applied 1-D thermodynamic sea ice growth model. Small dots represent individual point calculations
for the specific month and region, while the large filled circles represent monthly regional means. For snow ice, mean values
are calculated by taking the overall mean (filled), as well as the pure mean snow ice thickness, i.e., averaging only over the
cases where snow ice is actually present (open circles).

The Snow Buoy results underline that sea ice in the Weddell Sea is characterized by a year-round snow cover, highlighting the
dynamic nature of snow processes. The Weddell Sea region shows remarkable differences in annual net accumulation/ablation
patterns. In the central/northeastern (C/NE) Weddell Sea, an average net accumulation of 57 cm is observed, whereas in the
northwestern (NW) Weddell Sea a significantly lower accumulation of only 8 cm is observed (Figure 2A). However, when
considering the annual mean of the actual snow accumulation rate, which includes potential snow-to-ice conversion fractions,
the mean values range from 52 ± 31 cm/year in the southeastern (C/SE) region to 66 ± 41 cm and 68 ± 33 cm in the C/NE and
NW regions, respectively, and increase further to 74 ± 41 cm in the southwestern (SW) region (Figure 1B).

Examining individual time series of snow accumulation recorded by the Snow Buoys (Figure 3B/D) reveals that snow
accumulation takes place throughout the year driven by both continuous deposition and occasional events. Overall, the seasonal
cycle of net snow accumulation/ablation is generally modest for most regions (Figure 2A), which is in agreement with the
seasonal cycle of precipitation derived from reanalysis data in the region (e.g., Boisvert et al., 2020). However, the SW region
is dominated by perennial sea ice, and the associated limitations on buoy deployments, and thus data availability hinders a
comprehensive seasonal analysis (Figure 1A).

For the C/NE Weddell Sea, the period from May to December shows the largest monthly net snow accumulation (Figure 2A),
which can be attributed to its closer proximity to the ice edge, along with typical eastward-moving cyclone paths, causing
precipitation in the region (Boisvert et al., 2020). Also, the C/SE Weddell Sea experiences above average net snow
accumulation in October, which may be due to local topographic effects associated with, for example, the grounded iceberg
A23A. The iceberg acts as a barrier, blocking the westward movement of sea ice in the area, and thus influences snow
accumulation patterns towards significantly higher accumulation rates, as observed for Snow Buoys 2014S10 and 2014S12
(Nicolaus et al., 2021).

200   In contrast, significant snow depth reduction or melt is mainly observed during the summer months in the Marginal Ice Zone (MIZ), with monthly net snow mass loss/melt occurring exclusively in December and January. Here, a maximum snow loss of 15 cm / month is observed in the NW Weddell Sea in December, while the C/NE Weddell Sea experiences a loss of 4 cm in January. The C/SE region, however, exhibits a low ablation period between May and August, with an average loss of up to 3 cm / month. This phenomenon could be linked to snow compaction and redistribution caused by katabatic winds originating
205   from the east coast of the Weddell Sea (Venegas and Drinkwater, 2001).

The observed latitudinal patterns of snow mass loss in the Weddell Sea region are consistent with satellite radiometric analyses of seasonal snowmelt processes, indicating a consistent latitudinal gradient in the timing and intensity of snowmelt (Arndt et al., 2016; Willmes et al., 2009).

Based on the ~~presented~~ data from the 36 Snow Buoys, the Weddell Sea shows spatial and temporal variability in snow
210   accumulation and ablation, with particularly high accumulation rates in the predominantly perennial sea ice areas of the southern and western regions. Therefore, considering the hydrostatic equilibrium of sea ice, the question arises as to how much of the initially accumulated snow remains as snow until the end of the ice floe or buoy drift, and how much has been transformed into meteoric ice over time, which is addressed in the following section.

3.3 Seasonal transition of snow into snow ice

215   Considering the often-high snow accumulation rates presented in Section 3.2 and the hydrostatic equilibrium of sea ice, it becomes clear that not all of the snow that has fallen on sea ice remains snow. Instead, the snow is transformed into snow ice at the snow-ice interface. Thus, the snow accumulation does not equal snow depth, but has to be corrected for the snow ice fraction. To achieve this, a one-dimensional thermodynamic sea ice model is applied along the drift trajectories of each Snow Buoy, yielding both the thermodynamic sea ice growth or melt at the bottom and the snow ice formation at the top. The model
220   is forced with the sea ice thickness at the time of buoy deployments, the daily-averaged snow accumulation retrieved from the Snow Buoys, and the surface heat fluxes obtained from the ERA5 reanalysis data.

For the analysis of the resulting actual snow depth, it needs to be taken into account that most buoys were deployed on sea ice either during or towards the end of summer, making the ice floes at least one year old during the deployments. As a result, the mean snow depths primarily represent data from second-year sea ice. Additionally, some Snow Buoys drifted with the sea ice
225   for two years or more, resulting in a correspondingly aged snow regime. For example, Snow Buoy 2014S10 remained adrift ~~with the sea ice~~ for almost three years, leading to measured snow depths pertaining to the 2-to-4-year snow regime.

The results show that for 46% of the analyzed Snow Buoy tracks, i.e., 16 buoys, the model detected snow ice formation (Figure 1C). This was particularly the case for buoys deployed on the fast ice at the northeastern edge of the Weddell Sea, which then drifted with the Weddell Gyre, and for buoys in the western Weddell Sea, i.e., in the perennial ice regime. The mean maximum
230   thickness of snow ice for these 16 ice floes was 34 cm, which accounts for 27% of the snow accumulation. Taking the whole

data set, including ice floes without snow ice, the mean maximum snow ice thickness is 16 cm for the Weddell Sea (Figure 2B).

3.3.1 Eastern Weddell Sea
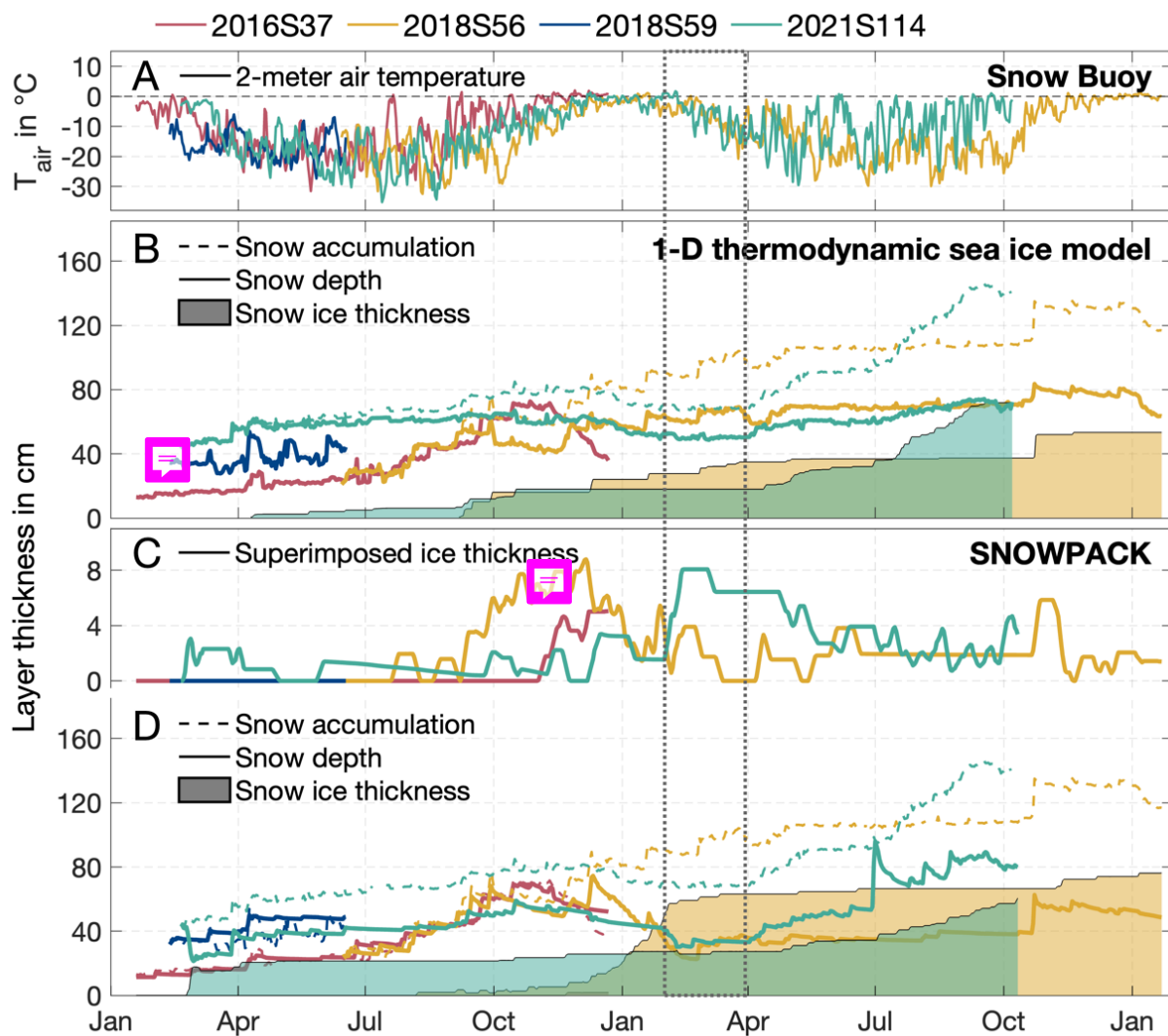
Figure 3. Time series of **A** 2-meter air temperature measured by the presented Snow Buoys and results from **B** the applied 1-D thermodynamic sea ice growth model and **C** and **D** the snow model SNOWPACK for layer thicknesses of the snow accumulation retrieved from the Snow Buoys (dashed lines) and the calculated snow depth (solid lines) and snow ice thickness (filled areas). The colors represent the four exemplary Snow Buoys 2016S37 (red), 2018S56 (yellow), 2018S59 (blue) and 2021S114 (green) (Figure 1). The data are plotted for the corresponding months, with the buoy deployment year indicated by

235

240   the buoy name (e.g., buoy 2016S37 is deployed in 2016). The dashed box across all panels indicates the time frame of the corresponding field data (Figure 1).

In the C/SE region, the maximum monthly mean snow ice thickness is reached in late spring, i.e., October, with an average of 35 ± 10 cm. This value coincides well with the time of maximum snow accumulation in the region, as shown in Figure 2A.

245   Furthermore, the calculated snow ice thickness in February/March was found to be 23 ± 15 cm, which is reasonably consistent with the observed snow ice thickness of 21 ± 18 cm, ranging from 0 to 58 cm, obtained from ice cores taken in the same region in 2021 (Figure 1A). However, only 14% of the Snow Buoy data points indicate potential snow ice formation in February/March (Figure 2B), while 84% of the analyzed ice cores (16 out of 19) confirm the presence of snow ice.

As many of the C/SE buoys continue to drift into the C/NE region (Figure 1C), it is expected that the snow ice layer will

250   continue to develop in this area, given the ~~ongoing~~ snow accumulation (Figure 2A), resulting in an average maximum monthly areal snow ice thickness of 41 ± 1 cm in early autumn, i.e., March and April. These large thicknesses are attributed to both the origin of the ice floes (C/SE Weddell Sea) and the lower sea ice concentration combined with higher surface energy fluxes, both of which are attributed to the lower latitudes leading to a warming of the upper ocean and consequent melting of the sea ice bottom. As a result, the potential for flooding and snow ice formation remains high.

255   Correcting the snow accumulation for the calculated snow ice thickness reveals an even weaker seasonal cycle in snow depth compared to the snow accumulation rates discussed before (Section 2.2), especially in the C/NE Weddell Sea. Here, the highest monthly mean of 62 cm is observed in December and the lowest monthly mean of 45 cm in July (Figure 2C). In contrast, the C/SE Weddell Sea shows the highest snow depth in November and the lowest in February, with mean values of 70 cm and 30 cm, respectively (Figure 2C). For the months of February/March, the corrected mean snow depth values of 33 ± 22 cm agree

260   well with the measured snow depths of 35 ± 23 cm on average during the *RV Polarstern* expedition PS124 in 2021. The C/SE Weddell Sea is not significantly impacted by additional internal processes such as superimposed ice formation (Arndt, 2022; Nicolaus et al., 2009), due to the high southern latitudes, the proximity to the continent, and associated cold katabatic winds (Ebner et al., 2014). Therefore, it can be concluded that the retrieved snow depth values for the C/SE Weddell Sea presented here correspond to the actual values and that the model parameters used appear to be ~~very appropriate for the region.~~

265   Considering that the southeastern Weddell Sea, due to the high southern latitudes and the proximity to the continent and the associated cold katabatic winds (Ebner et al., 2014), is hardly influenced by further hidden internal processes, such as superimposed ice formation, it can be concluded that the retrieved snow depth values for the SE Weddell Sea, as presented here, correspond to the actual values, and the model parameters used for the region appear to be highly appropriate.

3.3.2 Western Weddell Sea

270 For the SW Weddell Sea, the highest snow ice layer thicknesses are obtained in October and November with 29 ± 11 and 36 ± 8 cm, respectively (Figure 2C). For the NW Weddell Sea, the maximum monthly mean snow ice thickness is observed in July with 35 cm.

However, these monthly mean values for the region are not statistically significant as they are based on only 29 and 24 (SW) and 4 data points (NW) from ~~only one~~ buoy, respectively (Figure 2C). Nevertheless, the data are important to demonstrate the

275 potential for the thickest snow ice layers to occur in the western Weddell Sea, i.e., that most snow is converted to snow ice in the predominantly perennial sea ice regime. This is also supported by observations made in February/March 2022 in the region during the Endurance22 expedition (Rabenstein, 2022). Using ice core data, from which snow, meteoric ice and thermodynamically grown ice can be distinguished by salinity and stable water isotope analyses, snow ice thicknesses between 2 and 89 cm were determined, with a mean value of 38 ± 24 cm, which ~~supports~~ the modelled snow ice thicknesses.

280 However, when considering the snow ice thicknesses calculated along the trajectory of Snow Buoy 2021S114 in February/March 2022 (Figure 1C), which was approximately 100 km away from the ice stations of the concurrent Endurance22 expeditions, the model gives a mean snow ice thickness of only 12 cm, i.e., one third of the measured layer thickness (Figure 3B). This discrepancy can be attributed to two possible causes: First, Nicolaus et al. (2021) showed that snow accumulation rates can vary considerably on spatial scales smaller than 250 km. Thus, the Snow Buoy may have experienced significantly

285 lower snow accumulation than the sampled ice floes of the Endurance22 expedition, despite similar atmospheric conditions. In addition, Snow Buoys are usually deployed on level ice and therefore do not account for snow drifting and accumulating in ice ridges. Thus, the Snow Buoy data may have a bias towards underestimating snow accumulation. Second, the thermodynamic sea ice model used here assumes a constant ocean heat flux. During spring/summer 2022, the sea ice edge was further south than usual (e.g., Turner et al., 2022), raising the possibility of a higher ocean heat flux, resulting in more bottom

290 sea ice melting and subsequently more potential for flooding and snow ice formation. Thus, doubling the ocean heat flux from 3 to 6 Wm^{-2}, the modelled snow ice thickness for the ice floe of Snow Buoy 2021S114 increases by 6 cm, highlighting the high sensitivity of the calculations to the ocean heat flux, especially in the marginal ice zone.

This discrepancy continues in the actual snow depths calculated: while the model calculates a mean snow depth in the NW Weddell Sea of 35 ± 19 cm and 33 ± 18 cm for February and March (Figure 2D), respectively, the field measurements reveal

295 a snow depth of 15 ± 11 cm (Rabenstein, 2022). It is important to highlight that the ice floes and Snow Buoys present in the region are at least three, and in some cases, even four years old. As a result, the measured snow depths represent the corresponding perennial snow layers, a common occurrence in the region (Melsheimer et al., 2023). This is evident from the calculated maximum snow depths of 81 and 93 cm observed between August and November in the western Weddell Sea (Figure 2D). Therefore, in order to compile a complete snow climatology for the region, the snow depth values presented here

300 must be assigned to corresponding ice age classes, which is beyond the scope of this study.

The calculated snow depths presented here correct the snow accumulation only for snow ice formation but do not consider other snow-to-ice conversion processes, such as superimposed ice formation, or sublimation. These additional processes decrease snow depth even more in this relatively northern region with elevated surface energy fluxes (Nicolaus et al., 2006; Arndt et al., 2021), and will be discussed in detail in the following Section 3.4.

3.4 Quantitative impact of snow metamorphism on the actual snow depth

The one-dimensional thermodynamic sea ice model used allows the description of the snow-to-ice conversion process by adjusting the snow-ice interface, maintaining the hydrostatic equilibrium of the sea ice and its snow cover. However, air temperature measurements from the analyzed Snow Buoys show temporary occurrences of temperatures around the freezing point (Figure 3A), especially during the summer season. This suggests the possibility of internal snow melting followed by refreezing, leading to the formation of superimposed ice. In order to quantitatively assess the contribution of superimposed ice, the snow model SNOWPACK was used in a simplified configuration, excluding wind-driven snow drift processes. In this context, 50% of the data points have superimposed ice thickness calculated, which is characterized by an average maximum layer thickness of 6 ± 4 cm per buoy track (Figure 4A). However, the analysis excludes Snow Buoy 2014S10 due to its maximum superimposed ice thickness of 32 cm, which is an outlier caused by an extended period spent ~~in highly~~ northern latitudes (Nicolaus et al., 2021). Also Snow Buoys 2014S9 and 2014S12 spent a considerable amount of time in the northern latitudes with snow accumulations of up to 120 cm, resulting in a maximum superimposed ice thickness of 14 cm. For all other buoys, the thickness of the maximum superimposed ice layer ranges between 2 and 9 cm, with a tendency towards thicker layers at more northern latitudes and thinner layers or no superimposed ice south of 70°S (Figure 4A).

The findings presented here agree with superimposed ice observations during recent expeditions to the Weddell Sea: Though the ice core analysis from PS124 expedition conducted in March 2021 did not detect any superimposed ice in the southeastern Weddell Sea, the same ice regime that moved into the northwestern Weddell Sea in March 2022 showed an average thickness ~~of superimposed ice layer~~ of 8 ± 5 cm, varying from 0 to 17 cm (Haas et al., 2021; Rabenstein, 2022). Also the ice regime in the northwestern Weddell Sea originating from the southwest shows a mean superimposed ice thickness of 11 ± 11 cm at the end of summer 2019 (Arndt et al., 2021). Both, observations and snow model results, indicate that the thickness of the superimposed ice layer displays a latitude-dependent gradient. This is in agreement with the internal snowmelt onset calculated using passive and active microwave satellite data. The results show that the detection of seasonal internal melt-freeze cycles occurs earlier at more northern locations: the more northern the location, the earlier the detection of seasonal internal melt-freeze cycles (Arndt and Haas, 2019; Arndt et al., 2016). These processes correlate with the latitude-dependent surface energy fluxes.

The latitude-dependent superimposed ice formation is also reflected in the comparison of snow depths between the one-dimensional sea ice model and the SNOWPACK model (Figure 4B), where the actual snow depth tends to be thinner because

not only the snow ice but also the superimposed ice formation is taken into account. This is particularly the case for buoys 2018S56 and 2021S114 that have been drifting for a long time in more northern latitudes and have ~~experienced therefore~~ more melting. These results demonstrate the potential of using snow models to reduce uncertainties in estimating snow depth from

335 snow accumulation data on Antarctic sea ice. However, processes such as snow redistribution by drift processes are not yet included – a requirement that, in combination with the snow-to-ice conversion processes discussed here, will play an important role in the development of future snow models on sea ice in order to be able to close the snow mass budget on Antarctic sea ice.
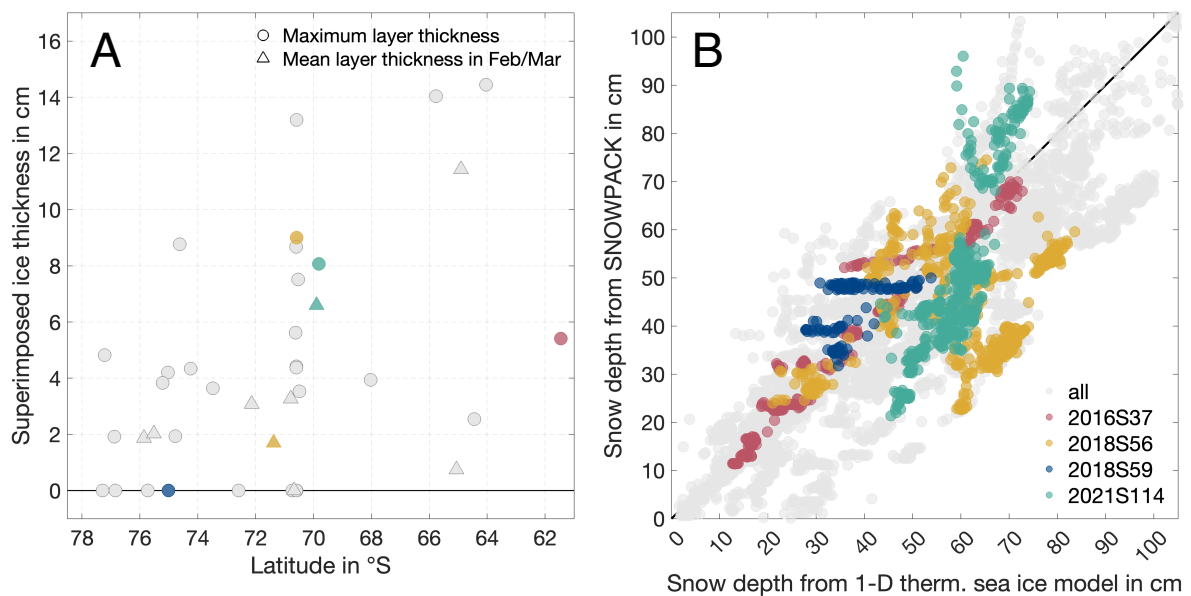
340 **Figure 4. A** Maximum layer thickness over the whole time series (circles) and mean layer thickness over the February to March period of superimposed ice as a function of latitude. **B.** Correlation of snow depth estimates obtained by the one-dimensional sea ice model (x-axis) and SNOWPACK (y-axis). The diagonal line represents perfect agreement between the two models. Grey markers represent the respective calculations for all Snow Buoys, while colored markers represent the four exemplary Snow Buoys 2016S37 (red), 2018S56 (yellow), 2018S59 (blue) and 2021S114 (green) (Figure 1).

345 **4 Summary and Conclusion**

In this study, we used a comprehensive snow accumulation dataset acquired from Snow Buoys deployed on level ice drifting in the Weddell Sea over the last decade. Our primary objective was to derive the actual snow depth from snow accumulation and surface elevation data. This was achieved by assessing snow ice layer thicknesses along the drift trajectories using a one-dimensional thermodynamic sea ice model. In addition, we incorporated the snow model SNOWPACK to account for key

350 snow metamorphism processes, including the formation of superimposed ice.

Our results ~~emphasize~~ that snow ice formation takes place primarily in the eastern Weddell Sea. In this region, the combination of sea ice growth at the snow/ice interface through snow-to-ice conversion processes and the insulating properties of snow act as a barrier to significant thermodynamic growth during the winter months. Thus, as it drifts towards the northwestern Weddell Sea, the rather thick sea ice limits the formation of additional snow ice during the winter season. However, the potential for

355 snow ice formation returns in summer, driven by the onset of bottom melt and increased snowfall, particularly in response to the influx of warmer, moister air masses towards the ice edge. As a result, our analysis shows that the thickest snow ice layers within the perennial sea ice zones of the northwestern Weddell Sea are those originating from the southeastern Weddell Sea. This phenomenon is due to the balancing effects of hydrostatic equilibrium, which maintain a consistent snow layer thickness even in regions characterized by high snow accumulation rates, such as the southwestern Weddell Sea, or during localized

360 instances of intense snowfall where large amounts of snow ice are formed.

The evidence of current declining sea ice extent in the Southern Ocean suggests the possibility of increased ocean heat fluxes in the coming years and decades (e.g., Eayrs et al., 2021; Purich and Doddridge, 2023). These changes could lead to increased rates of bottom sea ice melt, increasing the likelihood of flooding and associated snow ice formation. At the same time, warmer air temperatures are expected to allow for higher moisture content, leading to increased snowfall and hence increased potential

365 for flooding and snow ice formation. Concurrently, however, warming air temperatures and the associated shift in the surface energy fluxes above the sea ice may also increase snow mass loss through surface melting. This metamorphic and wet snow reduces the albedo and eventually leads to an ice-albedo feedback-supported appearance of melt ponds caused by more Arctic-like atmospheric conditions, which is referred to as "Arctification" of the Antarctic sea ice (Arndt et al., 2021).

In conclusion, this study underscores the critical importance of understanding snow transformation processes, not only under

370 current conditions, but also in anticipation of future changes in the coupled Antarctic sea ice system. Hidden processes will remain hidden, while large-scale analyses will have increasing importance, based on model and satellite remote sensing data. It is imperative to further develop and refine existing snow models to better reflect Antarctic sea ice conditions. This will enable us to close the Antarctic snow mass budget and improve the estimates of Antarctic sea ice thickness derived from both sea ice modelling and satellite remote sensing applications. A full understanding of these processes is essential to capture the

375 complex dynamics of the Antarctic sea ice environment and its response to ongoing climate change.

Data availability

Snow accumulation measurements from Snow Buoys were obtained from https://www.meereisportal.de (grant: REKLIM-2013-04) and are stored in PANGAEA (Nicolaus et al., 2021, https://doi.pangaea.de/10.1594/PANGAEA.875638).
All ERA5 data from ECMWF are accessed and downloaded from the Copernicus Climate Change Service (last access: 29

380 September 2023): https://cds.climate.copernicus.eu/cdsapp#!/dataset/reanalysis-era5-single-levels?tab=form.

All snow depth data from ice station work are available at https://doi.org/10.1594/PANGAEA.946183 (Arndt, 2022), https://doi.pangaea.de/10.1594/PANGAEA.928966 (Arndt & Haas, 2021), and https://doi.pangaea.de/10.1594/PANGAEA.946177 (Arndt & Haas, 2022).

MeteoIO and SNOWPACK are software published under a GNU LGPLv3 license by the WSL Institute for Snow and
385 Avalanche Research SLF at https://gitlabext.wsl.ch/snow-models. The model source code used in this study was downloaded on 26 April 2023.

Authors contribution

SA and MN coordinated the deployment of the Snow Buoys in the Weddell Sea. SA set up and performed the one-dimensional thermodynamic sea ice model, while NM and LR set up and performed the SNOWPACK model runs. SA performed all
390 analyses and prepared the figures for the paper. All authors contributed to discussions and the actual writing.

Competing interests

The authors declare that they have no conflict of interest.

Acknowledgements

We gratefully acknowledge the support of the cruise leaders, all involved scientists, the helicopter teams on board, and the
395 captains and crews of *R/V Polarstern* during expeditions PS81, PS82, PS89, PS96, PS103, PS111, and PS124 (grant numbers AWI_PS81_00, AWI_PS82_02, AWIPS89_02, AWI_PS96_01, AWI_PS103_02, AWI_PS111_00, AWI_PS124_08). In the same way, we acknowledge the work of all people involved of the Endurance22 expedition with the *S.A. Agulhas II*. Furthermore, we acknowledge all wintering teams at Neumayer Station III supporting the regular deployment of buoys in Atka Bay near the base. We highly appreciate the work of the www.meereisportal.de team for building and maintaining the online
400 platform and database for all Snow Buoy data (REKLIM-2012-04).

Financial support

This work received funding from the German Research Foundation's (DFG) projects fAntasie (AR1236/3-1), SnowCast (AR1236/1-1), SCASI (NI1096/5-1) and SCASI-RS (MA 5056/2-1) within its priority program "Antarctic Research with comparative investigations in the Arctic ice areas" (SPP1158), the DFG Emmy Noether Programme project SNOWflAke
405 (project number 493362232), the University of Hamburg, and the Alfred-Wegener-Institut, Helmholtz-Zentrum für Polar- und Meeresforschung. All buoys were funded by the Helmholtz infrastructure programmes ACROSS and FRAM with contributions for data transmission by the German Weather service (DWD) and the International Arctic Buoy Program (IABP).

References

Ackley, S., Lewis, M., Fritsen, C., and Xie, H.: Internal melting in Antarctic sea ice: Development of "gap layers", Geophysical
410 Research Letters, 35, https://doi.org/10.1029/2008GL033644, 2008.

Arndt, S., Willmes, S., Dierking, W., and Nicolaus, M.: Timing and regional patterns of snowmelt on Antarctic sea ice from
passive microwave satellite observations, Journal of Geophysical Research - Oceans, 121, 5916-5930,
10.1002/2015JC011504, 2016.

Arndt, S., and Haas, C.: Spatiotemporal variability and decadal trends of snowmelt processes on Antarctic sea ice observed by
415 satellite scatterometers, The Cryosphere, 13, 1943-1958, 10.5194/tc-13-1943-2019, 2019.

Arndt, S., Hoppmann, M., Schmithüsen, H., Fraser, A. D., and Nicolaus, M.: Seasonal and interannual variability of landfast
sea ice in Atka Bay, Weddell Sea, Antarctica, The Cryosphere, 14, 2775-2793, 10.5194/tc-14-2775-2020, 2020.

Arndt, S., Haas, C., Meyer, H., Peeken, I., and Krumpen, T.: Recent observations of superimposed ice and snow ice on sea ice
in the northwestern Weddell Sea, The Cryosphere, 15, 4165-4178, 10.5194/tc-15-4165-2021, 2021.

420 Arndt, S.: Sensitivity of Sea Ice Growth to Snow Properties in Opposing Regions of the Weddell Sea in Late Summer,
Geophysical Research Letters, 49, e2022GL099653, https://doi.org/10.1029/2022GL099653, 2022.

Bartelt, P., and Lehning, M.: A physical SNOWPACK model for the Swiss avalanche warning: Part I: numerical model, Cold
Regions Science and Technology, 35, 123-145, 2002.

Boisvert, L. N., Webster, M. A., Petty, A. A., Markus, T., Cullather, R. I., and Bromwich, D. H.: Intercomparison of
425 precipitation estimates over the Southern Ocean from atmospheric reanalyses, Journal of Climate, 33, 10627-10651, 2020.

Calonne, N., Flin, F., Morin, S., Lesaffre, B., du Roscoat, S. R., and Geindreau, C.: Numerical and experimental investigations
of the effective thermal conductivity of snow, Geophysical Research Letters, 38, 10.1029/2011gl049234, 2011.

Copernicus Climate Change Service: ERA5: Fifth generation of ECMWF atmospheric reanalyses of the global climate,
https://cds.climate.copernicus.eu/cdsapp#!/home, 2017.

430 Eayrs, C., Li, X., Raphael, M. N., and Holland, D. M.: Rapid decline in Antarctic sea ice in recent years hints at future change,
Nature Geoscience, 14, 460-464, 10.1038/s41561-021-00768-3, 2021.

Ebner, L., Heinemann, G., Haid, V., and Timmermann, R.: Katabatic winds and polynya dynamics at Coats Land, Antarctica,
Antarct Sci, 26, 309-326, 2014.

Eicken, H., Lange, M. A., Hubberten, H. W., and Wadhams, P.: Characteristics and distribution patterns of snow and meteoric
435 ice in the Weddell Sea and their contribution to the mass balance of sea ice, Annales Geophysicae-Atmospheres Hydrospheres
and Space Sciences, 12, 80-93, 10.1007/s00585-994-0080-x, 1994.

Fons, S. W., and Kurtz, N. T.: Retrieval of snow freeboard of Antarctic sea ice using waveform fitting of CryoSat-2 returns,
The Cryosphere, 13, 861-878, 2019.

Grosfeld, K., Treffeisen, R., Asseng, J., Bartsch, A., Bräuer, B., Fritzsch, B., Gerdes, R., Hendricks, S., Hiller, W., and
440 Heygster, G.: Online sea-ice knowledge and data platform < www. meereisportal. de >, Polarforschung, 85, 143-155, 2015.

Haas, C., and Eicken, H.: Interannual variability of summer sea ice thickness in the Siberian and central Arctic under different atmospheric circulation regimes, Journal of Geophysical Research: Oceans, 106, 4449-4462, 2001.

Haas, C., Nicolaus, M., Willmes, S., Worby, A., and Flinspach, D.: Sea ice and snow thickness and physical properties of an ice floe in the western Weddell Sea and their changes during spring warming, Deep-Sea Res Pt Ii, 55, 963-974, 10.1016/J.Dsr2.2007.12.020, 2008.

Haas, C., Arndt, S., Peeken, I., and Allhusen, E.: Chapter Sea Ice in: The Expedition PS118 of the Research Vessel POLARSTERN to the Weddell Sea in 2019, Berichte zur Polar-und Meeresforschung= Reports on polar and marine research, 735, 97-123, 10.2312/BzPM_0735_2019, 2019.

Haas, C., Arndt, S., Peeken, I., Eggers, S. L., and Neudert, M.: Chapter Sea Ice Geophysics and Biogeochemistry in: The Expedition PS124 of the Research Vessel POLARSTERN to the Weddell Sea in 2021, Berichte zur Polar-und Meeresforschung= Reports on polar and marine research, 2021.

Harms, S., Fahrbach, E., and Strass, V. H.: Sea ice transports in the Weddell Sea, Journal of Geophysical Research: Oceans, 106, 9057-9073, https://doi.org/10.1029/1999JC000027, 2001.

Holtslag, A., and De Bruin, H.: Applied modeling of the nighttime surface energy balance over land, Journal of Applied Meteorology and Climatology, 27, 689-704, 1988.

Kottmeier, C., Olf, J., Frieden, W., and Roth, R.: Wind forcing and ice motion in the Weddell Sea region, Journal of Geophysical Research: Atmospheres, 97, 20373-20383, 1992.

Kottmeier, C., and Sellmann, L.: Atmospheric and oceanic forcing of Weddell Sea ice motion, Journal of Geophysical Research: Oceans, 101, 20809-20824, 1996.

Kwok, R., and Kacimi, S.: Three years of sea ice freeboard, snow depth, and ice thickness of the Weddell Sea from Operation IceBridge and CryoSat-2, The Cryosphere, 12, 2789-2801, 2018.

Kwok, R., Kacimi, S., Webster, M., Kurtz, N., and Petty, A.: Arctic snow depth and sea ice thickness from ICESat-2 and CryoSat-2 freeboards: A first examination, Journal of Geophysical Research: Oceans, 125, e2019JC016008, 2020.

Lehning, M., Bartelt, P., Brown, B., and Fierz, C.: A physical SNOWPACK model for the Swiss avalanche warning Part III: meteorological forcing, thin layer formation and evaluation, Cold Regions Science and Technology, 35, 169-184, 2002a.

Lehning, M., Bartelt, P., Brown, B., Fierz, C., and Satyawali, P.: A physical SNOWPACK model for the Swiss avalanche warning: Part II. Snow microstructure, Cold regions science and technology, 35, 147-167, 2002b.

Massom, R., Eicken, H., Haas, C., Jeffries, M. O., Drinkwater, M. R., Sturm, M., Worby, A. P., Wu, X. R., Lytle, V. I., Ushio, S., Morris, K., Reid, P. A., Warren, S. G., and Allison, I.: Snow on Antarctic Sea ice, Rev Geophys, 39, 413-445, 10.1029/2000rg000085, 2001.

Melsheimer, C., Spreen, G., Ye, Y., and Shokr, M.: First results of Antarctic sea ice type retrieval from active and passive microwave remote sensing data, The Cryosphere, 17, 105-126, 10.5194/tc-17-105-2023, 2023.

Nicolaus, M., Haas, C., Bareiss, J., and Willmes, S.: A model study of differences of snow thinning on Arctic and Antarctic first-year sea ice during spring and summer, Annals of Glaciology, 44, 147-153, 10.3189/172756406781811312, 2006.

475 Nicolaus, M., Haas, C., and Willmes, S.: Evolution of first-year and second-year snow properties on sea ice in the Weddell Sea during spring-summer transition, Journal of Geophysical Research, 114, 10.1029/2008JD011227, 2009.

Nicolaus, M., Hoppmann, M., Arndt, S., Hendricks, S., Katlein, C., Nicolaus, A., Rossmann, L., Schiller, M., and Schwegmann, S.: Snow Depth and Air Temperature Seasonality on Sea Ice Derived From Snow Buoy Measurements, Frontiers in Marine Science, 8, 10.3389/fmars.2021.655446, 2021.

480 Paul, S., Willmes, S., and Heinemann, G.: Long-term coastal-polynya dynamics in the southern Weddell Sea from MODIS thermal-infrared imagery, The Cryosphere, 9, 2027-2041, 10.5194/tc-9-2027-2015, 2015.

Paul, S., Hendricks, S., Ricker, R., Kern, S., and Rinne, E.: Empirical parametrization of Envisat freeboard retrieval of Arctic and Antarctic sea ice based on CryoSat-2: progress in the ESA Climate Change Initiative, The Cryosphere, 12, 2437-2460, 10.5194/tc-12-2437-2018, 2018.

485 Purich, A., and Doddridge, E. W.: Record low Antarctic sea ice coverage indicates a new sea ice state, Communications Earth & Environment, 4, 314, 10.1038/s43247-023-00961-9, 2023.

Rabenstein, L.: Endurance22, Cruise Scientific Report, 1–95, 2022.

Ricker, R., Hendricks, S., Perovich, D. K., Helm, V., and Gerdes, R.: Impact of snow accumulation on CryoSat-2 range retrievals over Arctic sea ice: An observational approach with buoy data, Geophysical Research Letters, 42, 4447-4455, 2015.

490 Robertson, R., Padman, L., and Egbert, G. D.: Tides in the Weddell Sea, Ocean, Ice and Atmosphere: Interactions at the Antarctic Continental Margin, Antarct. Res. Ser, 75, 341-369, 1998.

Schwegmann, S., Haas, C., Fowler, C., and Gerdes, R.: A comparison of satellite-derived sea-ice motion with drifting-buoy data in the Weddell Sea, Antarctica, Annals of Glaciology, 52, 103-110, 10.3189/172756411795931813, 2011.

Schwegmann, S., Rinne, E., Ricker, R., Hendricks, S., and Helm, V.: About the consistency between Envisat and CryoSat-2 495 radar freeboard retrieval over Antarctic sea ice, Cryosphere, 9, 4893-4923, 10.5194/tc-10-1415-2016, 2016.

Spreen, G., Kaleschke, L., and Heygster, G.: Sea ice remote sensing using AMSR-E 89-GHz channels, Journal of Geophysical Research-Oceans, 113, 10.1029/2005jc003384, 2008.

Sturm, M., Holmgren, J., Konig, M., and Morris, K.: The thermal conductivity of seasonal snow, Journal of Glaciology, 43, 26-41, 1997.

500 Sturm, M., and Holmgren, J.: An automatic snow depth probe for field validation campaigns, Water Resources Research, 54, 9695-9701, 2018.

Thorndike, A.: A toy model linking atmospheric thermal radiation and sea ice growth, Journal of Geophysical Research: Oceans, 97, 9401-9410, 1992.

Tian, L. J., Gao, Y. L., Weissling, B., and Ackley, S. F.: Snow-ice contribution to the structure of sea ice in the Amundsen 505 Sea, Antarctica, Annals of Glaciology, 61, 369-378, 10.1017/aog.2020.55, 2020.

Turner, J., Holmes, C., Caton Harrison, T., Phillips, T., Jena, B., Reeves-Francois, T., Fogt, R., Thomas, E. R., and Bajish, C.: Record low Antarctic sea ice cover in February 2022, Geophysical Research Letters, 49, e2022GL098904, 2022.

Venegas, S. A., and Drinkwater, M. R.: Sea ice, atmosphere and upper ocean variability in the Weddell Sea, Antarctica, Journal of Geophysical Research-Oceans, 106, 16747-16765, Doi 10.1029/2000jc000594, 2001.

510   Vernet, M., Geibert, W., Hoppema, M., Brown, P. J., Haas, C., Hellmer, H., Jokat, W., Jullion, L., Mazloff, M., and Bakker, D.: The Weddell Gyre, Southern Ocean: present knowledge and future challenges, Rev Geophys, 57, 623-708, 2019.

Vihma, T., Launiainen, J., and Uotila, J.: Weddell Sea ice drift: Kinematics and wind forcing, Journal of Geophysical Research: Oceans, 101, 18279-18296, https://doi.org/10.1029/96JC01441, 1996.

Webster, M., Gerland, S., Holland, M. M., Hunke, E., Kwok, R., Lecomte, O., Massom, R., Perovich, D., and Sturm, M.: Snow
515   in the changing sea-ice systems, Nature Climate Change, 1, 2018.

Wever, N., Schmid, L., Heilig, A., Eisen, O., Fierz, C., and Lehning, M.: Verification of the multi-layer SNOWPACK model with different water transport schemes, The Cryosphere, 9, 2271-2293, 10.5194/tc-9-2271-2015, 2015.

Wever, N., Würzer, S., Fierz, C., and Lehning, M.: Simulating ice layer formation under the presence of preferential flow in layered snowpacks, The Cryosphere, 10, 2731-2744, 10.5194/tc-10-2731-2016, 2016.

520   Wever, N., Rossmann, L., Maaß, N., Leonard, K. C., Kaleschke, L., Nicolaus, M., and Lehning, M.: Version 1 of a sea ice module for the physics-based, detailed, multi-layer SNOWPACK model, Geoscientific Model Development, 13, 99-119, 2020.

Wever, N., Leonard, K., Maksym, T., White, S., Proksch, M., and Lenaerts, J. T.: Spatially distributed simulations of the effect of snow on mass balance and flooding of Antarctic sea ice, Journal of Glaciology, 1-19, 2021.

Willmes, S., Haas, C., Nicolaus, M., and Bareiss, J.: Satellite microwave observations of the interannual variability of
525   snowmelt on sea ice in the Southern Ocean, Journal of Geophysical Research-Oceans, 114, 10.1029/2008jc004919, 2009.

Worby, A. P., Geiger, C. A., Paget, M. J., Van Woert, M. L., Ackley, S. F., and DeLiberty, T. L.: Thickness distribution of Antarctic sea ice, Journal of Geophysical Research-Oceans, 113, 10.1029/2007jc004254, 2008.